Talanta 271 (2024) 125697

Contents lists available at ScienceDirect

Talanta

journal homepage: www.elsevier.com/locate/talanta

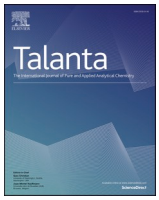

SERS-based detection of the antibiotic ceftriaxone in spiked fresh plasma and microdialysate matrix by using silver-functionalized silicon nanowire substrates

Chen Liu [a,b], Célia Franceschini [c], Susanne Weber [d], Tony Dib [a,b], Poting Liu [a,b], Long Wu [a,e,f], Edoardo Farnesi [a,b], Wen-shu Zhang [g], Vladimir Sivakov [a], Peter B. Luppa [d], Jürgen Popp [a,b], Dana Cialla-May [a,b,*]

[a] Leibniz Institute of Photonic Technology, Member of Leibniz Health Technologies, Member of the Leibniz Centre for Photonics in Infection Research (LPI), Albert-Einstein-Straße 9, 07745, Jena, Germany
[b] Institute of Physical Chemistry (IPC) and Abbe Center of Photonics (ACP), Friedrich Schiller University Jena, Member of the Leibniz Centre for Photonics in Infection Research (LPI), Helmholtzweg 4, 07743, Jena, Germany
[c] UR Molecular Systems, Department of Chemistry, University of Liège, 4000, Liège, Belgium
[d] Institute of Clinical Chemistry and Pathobiochemistry, Klinikum Rechts der Isar of the Technische Universität München, Ismaninger Str. 22, 81675, München, Germany
[e] School of Food Science and Engineering, Key Laboratory of Tropical and Vegetables Quality and Safety for State Market Regulation, Hainan University. Haikou 570228, China
[f] Key Laboratory of Fermentation Engineering (Ministry of Education), College of Bioengineering and Food, Hubei University of Technology, Wuhan, 430068, China
[g] China Fire and Rescue Institute, Beijing, 102202, China

ARTICLE INFO

Handling editor: Ian D McKelvie

Keywords:
TDM
Ceftriaxone
SERS
Silicon nanowires
Silver
Nanoparticles
Quantitative analysis
Fresh plasma
Microdialysate

ABSTRACT

Therapeutic drug monitoring (TDM) is an important tool in precision medicine as it allows estimating pharmacodynamic and pharmacokinetic effects of drugs in clinical settings. An accurate, fast and real-time determination of the drug concentrations in patients ensures fast decision-making processes at the bedside to optimize the clinical treatment. Surface-enhanced Raman spectroscopy (SERS), which is based on the application of metallic nanostructured substrates to amplify the inherent weak Raman signal, is a promising technique in medical research due to its molecular specificity and trace sensitivity accompanied with short detection times. Therefore, we developed a SERS-based detection scheme using silicon nanowires decorated with silver nanoparticles, fabricated by means of top-down etching combined with chemical deposition, to detect the antibiotic ceftriaxone (CRO) in spiked fresh plasma and microdialysis samples. We successfully detected CRO in both matrices with an LOD of 94 μM in protein-depleted fresh plasma and 1.4 μM in microdialysate.

1. Introduction

Therapeutic drug monitoring (TDM) is the process of determining drug concentrations in a patient's body fluid to identify the optimal dosing of a drug based on customized pharmacological models and therapeutic windows for individualized and precise treatment [1–3]. Therefore, the detection and quantification of drugs in TDM is an important foundation for rapid decision-making processes at the bedside. With accurate, rapid and real-time access to drug concentrations in patients, the clinical treatment protocol is most efficient.

Ceftriaxone (CRO) is a semi-synthetic cephalosporin, which is included in the World Health Organization's list of essential drugs [4]. Due to its broad spectrum and long half-life, CRO is effective in the treatment of infections caused by multi-drug resistant bacteria, such as upper respiratory tract infections and urinary tract infections. However, facing the widespread use of antibiotics and emergence of multi-drug resistant microorganisms, the development of tailored dosing regimens based on TDM has become an important tool to control antibiotic misuse, reduce toxic side effects and reduce drug-induced resistance in pathogens [5–7].

* Corresponding author. Leibniz Institute of Photonic Technology, Member of Leibniz Health Technologies, Member of the Leibniz Centre for Photonics in Infection Research (LPI), Albert-Einstein-Straße 9, 07745, Jena, Germany.
E-mail addresses: dana.cialla-may@leibniz-ipht.de, dana.cialla-may@uni-jena.de (D. Cialla-May).

https://doi.org/10.1016/j.talanta.2024.125697
Received 5 October 2023; Received in revised form 16 January 2024; Accepted 17 January 2024
Available online 18 January 2024
0039-9140/© 2024 Elsevier B.V. All rights reserved.

A high variety of analytical methods are available for TDM, where high-performance liquid chromatography coupled with mass spectrometry (HPLC-MS) is considered as "gold" standard [8]. CRO has been extensively studied as an important target in TDM employing typical HPLC systems [9–11]. However, HPLC-based methods have the disadvantages of being mostly restricted to core laboratories, requiring non-portable analytical equipment and trained personnel, and taking some analysis time also because of the sample preparation that is often required [12]. To allow for the estimation of the drug concentration in blood-based matrices of patients at the point-of-care, portable analytical methods need to be applied. As an example, Raman spectroscopy has proven to be available outside specialized laboratories by the development [13,14] and application of compact Raman spectrometers [15,16]. However, the sensitivity in Raman spectroscopy is not suited for low-concentrated analytes due to the inherent weak Raman effect. Therefore, plasmonic-active metallic nanostructures and nanoparticles are applied as active surfaces to enhance the Raman signal by 4–8 orders of magnitude, a technique which is known as surface-enhanced Raman spectroscopy (SERS) [17–20]. SERS is suited for food, biological and medical applications [21–23] due to its fast detection times enabled by signal enhancement, molecular specificity for fingerprint information as well as trace sensitivity allowing for the detection of targets in their relevant concentration range [24,25]. As a consequence, SERS is used in miniaturized portable assays and is particularly suitable for TDM applications at the point-of-care [1,3].

In clinical application schemes employing SERS for readout, procedures considering the characteristics of various human body fluids, such as urine, saliva or sweat secretions used as sample matrix for the detection of drug molecules, were developed [26–29]. In the case of blood plasma or serum, the presence of proteins in the sample is challenging as these biomolecules tend to form a corona around (metallic) nanoparticles which prevent the target analyte, i.e. antibiotic, to adsorb to the metallic sensor surface for an efficient Raman signal enhancement. Thus, the development of a direct SERS detection scheme of antibiotics in blood-derived matrices is confronted with the limitations due to the high protein content. In order to remove the interfering proteins, human blood-derived samples were pretreated by dilution with water [30], extraction by organic solvents [31] or solid phase microextraction [32], as well as proteins were precipitated by means of methanol [33]. Besides, microdialysis is an emerging technique based on the dialysis principle to remove larger biomolecules, such as proteins, by means of semi-permeable membranes with a defined low molecular weight cut-off [34,35]. This technique is available for TDM at the point-of-care, as the microdialysis probe inserted into the patient is perfused so that the analytes with a molecular weight below the membrane's cut-off diffuse in a concentration gradient-dependent manner through the membrane into the perfusion solution (=microdialysate) and are carried out by a continuous flow of perfusate in the dialysis tubing.

As illustrated in Fig. 1, the aim of this work was to apply the SERS analytical protocol to determine the antibiotic CRO in fresh plasma as well as in microdialysate as sample matrix to evaluate the best possible sample pretreatment for a SERS-based detection scheme. We applied SERS substrates which are based on silicon nanowires decorated with silver or gold nanoparticles and identified the best suited fabrication protocol to achieve sensitivity towards the lower μM concentration range. Finally, we applied our SERS-active sensor surface for the detection of CRO in spiked fresh plasma samples after protein precipitation and, in comparison, with the usage of microdialysates as complex matrix. We found an improvement of the limit of detection (LOD) from 94 μM in fresh plasma after protein precipitation to 1.4 μM in microdialysate samples.

2. Material and methods

The materials, instrumentation, formation of SERS substrates, preparation of blood-based samples, details about measurement conditions and data processing methods are described in Supporting Information.

3. Results and discussion

3.1. Spectral investigation of the antibiotic ceftriaxone (CRO)

Fig. 2A illustrates the Raman spectrum of the beta-lactam antibiotic CRO, which agreed with the previously published data [36,37]. The Raman mode at 757 cm^{-1} was identified as lactam ring breathing vibration, whereas the mode at 881 cm^{-1} and 1370 cm^{-1} was attributed to the C–N and carboxylate (COO^-) group vibration, respectively. Additionally, the mode at 1485 cm^{-1} was identified as the amide II vibration, and the Raman peak at 1570 cm^{-1} was due to the C=N stretching vibration. A detailed band assignment can be found in Table S1. In comparison, the SERS spectra of 1 mM CRO were recorded with arrays of silicon nanowires (SiNWs) decorated with either silver (Ag@SiNWs) or gold (Au@SiNWs) nanoparticles on top as SERS substrates (Fig. 2B).The schematic illustration of the fabrication process was depicted in Fig. S1. Here, it became obvious that the SERS and the Raman spectra differ in peak position and peak ratio, with higher SERS intensities using the Ag-decorated SERS substrates. We attributed this to the surface selection rules [38,39], i.e. Raman modes perpendicular to the metallic surface are preferentially enhanced, whereas those parallel to the surface are only weak or not detectable. Moreover, due to the evanescent character of the electromagnetic field on the SERS-active surface, only Raman modes in close vicinity (up to ~5 nm) to the sensing surface can contribute efficiently to the SERS spectrum [40]. As a consequence, for large (bio)molecules, the moieties that bind directly to the metal surface dominate the SERS spectrum in accordance to the surface selection rules. Under SERS conditions, the vibrational modes with the strongest

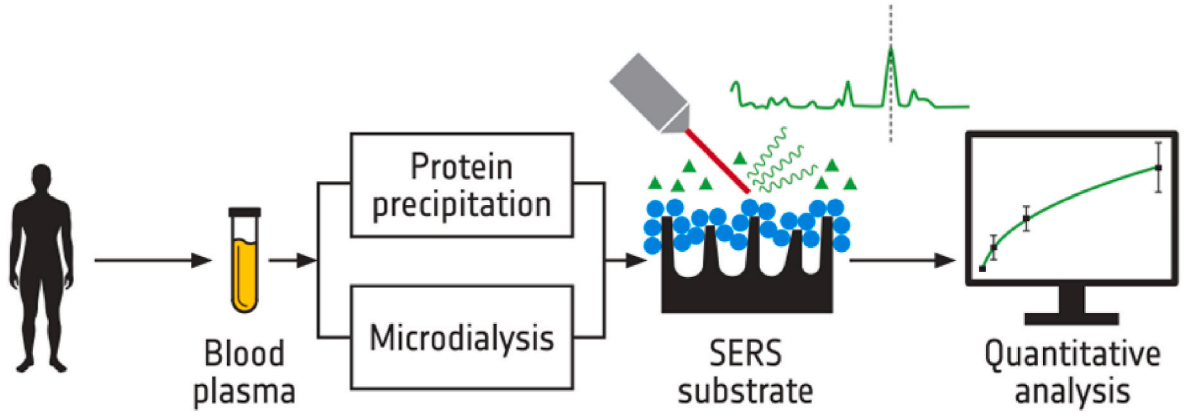

Fig. 1. Schematic illustration of SERS based detection strategy of CRO in human blood-derived samples.

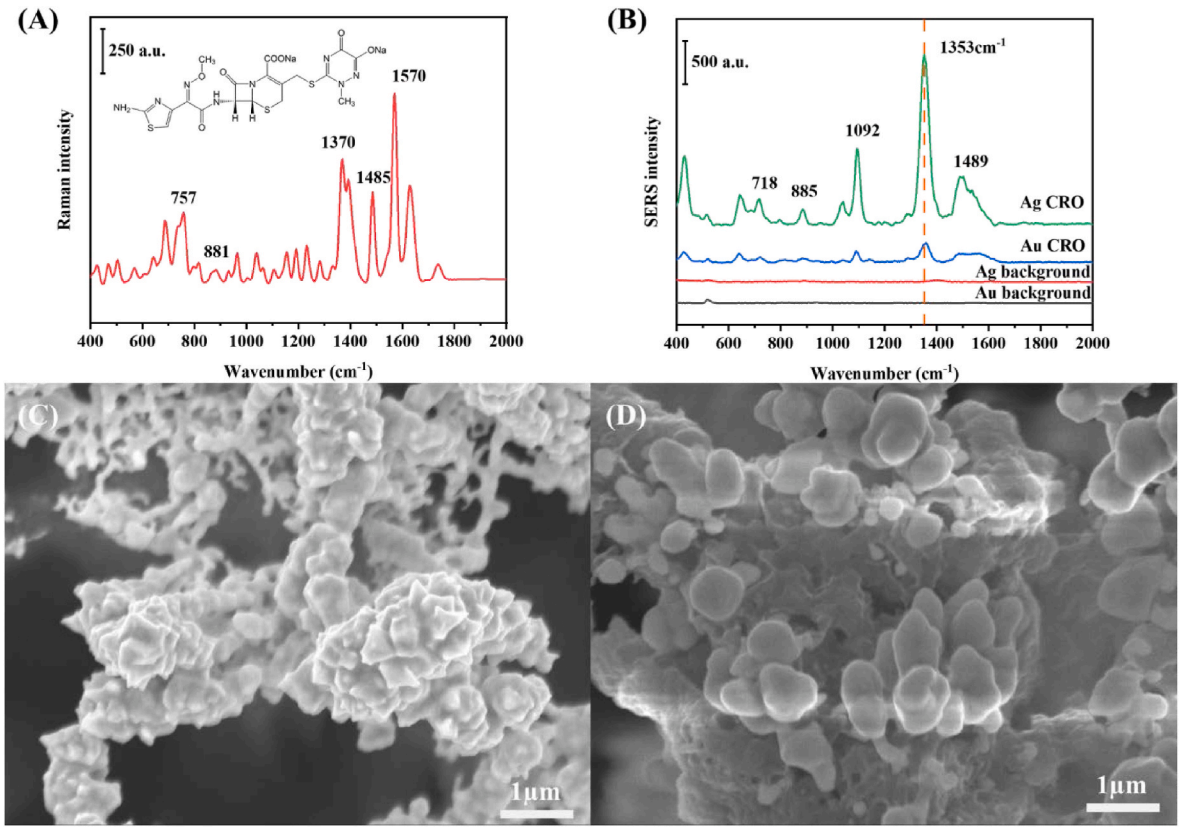

Fig. 2. (A) Raman spectrum of solid CRO, showing also the molecular structure of CRO; (B) SERS spectra of 1 mM CRO inclusively background signals, using Ag@SiNW (Ag) and Au@SiNW (Au) SERS substrates; (C–D) SEM images of the applied SERS substrates, i.e. SiNW after deposition with gold (C) or silver (D) applying a reaction time of 5 min. (For an explanation of the color references in this legend, the reader is referred to the online version of this paper.)

contributions to our recorded SERS spectrum corresponded to the carboxyl vibration at 1092 cm^{-1} and 1353 cm^{-1}, and the amide II vibration at 1489 cm^{-1}. From this observation we conclude that CRO was aligned perpendicular and the carboxyl group adjacent to the lactam ring was close to the surface of the nanoparticles. Consequently, we used the most intense vibrational mode under SERS conditions at 1353 cm^{-1} for the evaluation of the SERS intensity in further investigations. Within the background Raman signals of both applied SERS substrates only a Raman mode at approximately 520 cm^{-1} was detected (Fig. 2B), which arose from the first-order Raman modes in Si crystals [41,42].

As indicated above, the SERS enhancement effect of the Au@SiNWs substrate was obviously weaker than that of the Ag@SiNWs substrate (Fig. 2B). We propose that this was due to the different deposition process of the two metals. The SEM images in Fig. 2C and D shows that the growth of nanostructures on the gold substrate was denser, resulting in the formation of a more close and dense gold layer. In comparison, the dendrites on the silver substrate show a particle-like morphology. Due to the dense structure of the gold deposit only few nanogaps are observed in the SEM image, whereas in the case of silver nanostructures, a high number of nanogaps are observed, expected to act as hotspots in the SERS experiment. Based on the discussed results, we used the silver-based SERS substrates (Ag@SiNWs) for further experiments as they provided a higher SERS signal intensity.

3.2. Optimization of the SERS substrate fabrication process

In order to optimize the time for the deposition of the metal layer on the SERS substrates for maximum signal intensity, different silver deposition times (i.e. 1, 2, 5, 10, 15, 30, and 45 min) were tested. The SEM images were illustrated in Figs. S2 and S3 in Supporting Information, as well as the discussion of substrate characterization. The SERS substrates achieved after different deposition times were incubated for 30 min in an aqueous solution of 0.01 mM 4-MBA (used as model analyte). The SERS substrates were washed with deionized water to remove the excess molecules and the surface was dried under argon. Afterwards, SERS spectra were recorded. A total of three batches were tested per deposition time and three random areas (20 × 20 μm) of each substrate were scanned while measuring the SERS spectra. In doing so, 10 individual SERS spectra were obtained for each area of which the final average spectrum was calculated. Thus, for each deposition time, 90 individual SERS spectra were recorded. From the literature it is known that during the incubation process, 4-MBA forms a homogeneous layer on the surface of the substrate [43], which, when subjected to washing, effectively reduces the inhomogeneity of the adsorbed molecules. Fig. 3A and B shows the SERS spectra obtained from SERS substrates with different silver deposition times and the corresponding estimated peak areas at the characteristic Raman mode at 1070 cm^{-1}, which is due to the aromatic ring breathing [44]. With increasing silver deposition times, the SERS signal intensities increased to the highest signal at 5 min of silver deposition before they decrease again at higher deposition times. The relative standard deviation (SD) was approximately 19.6–57.8 %, which was dedicated to the inhomogeneity of the nanostructures across the surface of the SERS substrate as we fabricated them individually in several batches. It is expected that the observed inhomogeneity between the batches will be reduced once the fabrication can be performed in large scale with parallel fabrication of several tens or even hundreds of SERS-active substrates.

In order to allow for recording several scans under SERS conditions necessary for (semi-)quantitative assessment of drug concentrations within a timeframe of several 10 min after sample preparation, the SERS substrate stability needs to be confirmed. We investigated the stability of the Ag@SiNW SERS substrate signal after incubation with an aqueous

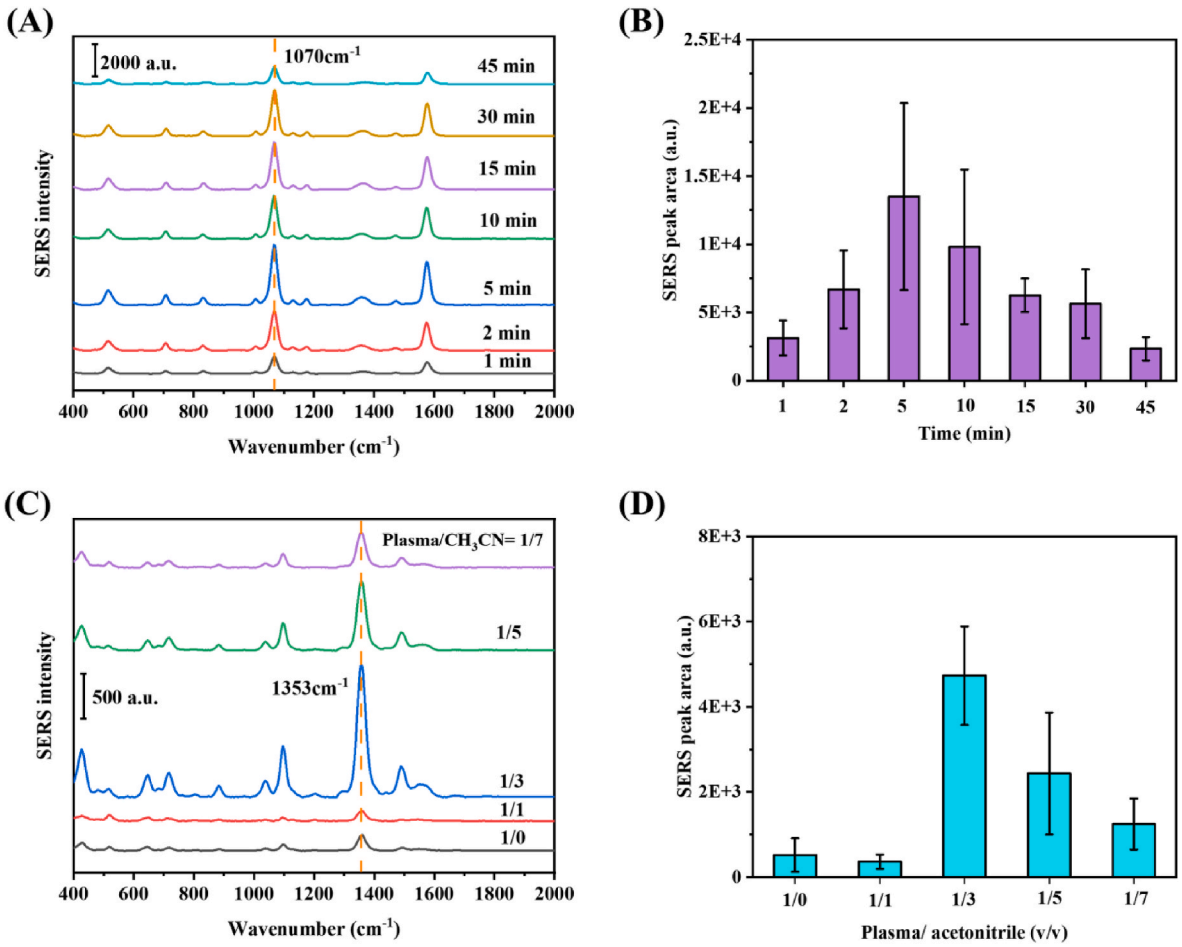

Fig. 3. (A) SERS spectra 0.01 mM 4-MBA in aqueous solution with silver deposition times of 1, 2, 5, 10, 15, 30 and 45 min. (B) Mean ± SD (bars) SERS spectrum peak areas at 1070 cm^{-1} in dependence of silver deposition times. Effect of protein precipitation using different plasma/acetonitrile ratios as sample pre-treatment on SERS spectra via Ag substrate were illustrated via Fig. 3C and D. (C) SERS spectra of 1 mM CRO-spiked plasma, pre-treated by protein precipitation using various protein/acetonitrile ratios. (D) Peak areas of the CRO marker mode at 1353 cm^{-1} for each plasma/acetonitrile.. (For an explanation of the color references in this legend, the reader is referred to the online version of this paper.)

CRO solution (0.25 mM) under ambient condition by analyzing the peak area of the CRO marker mode at 1353 cm^{-1} as function of SERS substrate storage time (Fig. S4). The first SERS spectra were measured directly after drying of the prepared sample-loaded SERS substrate, while the other four sets of SERS spectra were measured 15, 30, 45, and 60 min after drying and storage under ambient condition. For each storage conditions, 90 individual SERS spectra were recorded. Fig. S4 clearly shows that the peak areas at 1353 cm^{-1} did not differ significantly between the samples with different storage times. The similar peak areas implied that the sample-loaded SERS substrates were relatively stable and that they did not show significant deterioration, e.g. by oxide coverage of the substrate surface, or degradation of the test substance molecules on the substrate surface within the monitored period. Thus, the stability was sufficient to perform all required SERS measurements at the same conditions.

Due to the larger size of the silver nanoparticles when applying higher deposition time, the electromagnetic field coupling between nanostructures was reduced, leading to a reduction in the number of "hotspots", which was directly reflected in the reduction of the SERS signal intensity, as illustrated in Fig. 3A and B. Additionally, like previously published by Sivakov et al. [45], the crystallinity, crystals shape and size and surface chemical composition of obtained metal nanostructures during the galvanic displacement-based growth is strongly influenced by the deposition time. Consequently, the recorded SERS intensities decreased after 5 min silver deposition with increasing deposition time. Based on the results illustrated in Fig. 3A and B, we concluded that the highest SERS intensity was achieved for 5 min of silver deposition, which was applied for all further experiments. We additionally investigated the large area characteristic of the generated Ag@SiNW SERS substrates by SEM. The images showed that the uniformity of the applied substrates was acceptable in a large range, as illustrated by the micrometer scale in Fig. S5.

3.3. Protein precipitation protocol

To illustrate the potential of SERS in TDM, we performed SERS measurements with processed fresh plasma samples (protein-precipitated plasma supernatants and plasma microdialysates). Human plasma is an important biological fluid for individualized and tailored drug treatment, allowing the determination of the total but also the cell- and protein-unbound (free) drug concentrations in patient blood [35], which could be particularly important in critically ill patients with variable PK parameters. It consists of 90 % water and therein dissolved compounds such as plasma proteins, lipids, carbohydrates, inorganic salt ions, etc. [46], thus representing a quite complex sample matrix. The use of plasma in SERS measurements is challenging due to its high levels of the protein albumin (approximately 60 g L^{-1}). Albumin tends to adsorb onto the surface of SERS-active nanoparticles and thus to block the surface hot spots of the sensing surface, hinder the adsorption of the drug molecule of interest or cause surface degradation of solid phase

substrates when used as alternative to colloidal particles [30,47]. As a result, the performance of the SERS-based detection scheme is decreased and the necessity of removing proteins from fresh plasma as a sample pre-treatment step became obvious. One possible strategy is the precipitation of proteins in the sample matrix using the organic solvents, methanol and acetonitrile [48]. The use of methanol as protein precipitation reagent was already described for the SERS-based detection of methotrexate in human serum [33]. In pre-tests investigating various organic solvents for protein precipitation, we compared methanol and acetonitrile as protein precipitation reagents and observed that proteins appeared to precipitate after the addition of both solvents. Based on our observation, the protein precipitation in the methanolic phase was less dense than by using acetonitrile, which made it more difficult to separate the precipitate from the supernatant in the case of methanol, requiring also higher centrifugation speeds compared to acetonitrile. Therefore, acetonitrile was used as organic solvent in our following experiments.

For optimization of protein precipitation and SERS signal intensity, we mixed plasma samples spiked with final 1 mM CRO with acetonitrile in different ratios (i.e., 1/0, 1/1, 1/3, 1/5 and 1/7). Here, the ratio 1/0 corresponded to CRO-spiked plasma reference measurements without any protein precipitation. Fig. 3C and D shows the SERS spectra of CRO-spiked plasma supernatants after protein precipitation as well as the peak area of the CRO marker mode at 1353 cm^{-1} as function of the plasma/acetonitrile ratio. As illustrated, the best SERS signal was obtained at a plasma/acetonitrile ratio of 1/3, assuming that at this ratio interfering proteins were removed efficiently. In samples lacking protein precipitation (ratio 1/0) or with protein precipitation using a plasma/acetonitrile ratio of 1/1 only low SERS intensities were detected. This implied that the proteins of unprecipitated plasma blocked free binding sites and impeded the adsorption of CRO towards the SERS-active sensing surface. After addition of an equal volume of acetonitrile (ratio 1/1), it was assumed that CRO binding to proteins was abrogated by acetonitrile. However, because of the low extraction efficiency and insufficient protein precipitation due to the low total volume of organic solvent, this resulted in no significant change in the SERS signal. After the addition of organic solvent at 1/3, plasma proteins were efficiently precipitated and the SERS signal was significantly enhanced compared to the other conditions tested. At ratios of 1/5 and 1/7, although the increase in acetonitrile concentration improved the efficiency of protein precipitation, a significant decrease in SERS signals occurred due to the higher dilution of the analyte in the pre-treated sample caused by the higher volumes of the organic solvent. Therefore, a plasma/acetonitrile ratio of 1/3 was used for further measurements.

3.4. Quantitative analysis of ceftriaxone (CRO) in blood-based matrices

Our developed SERS-based protocol was next used to investigate the capabilities on estimating the concentration of CRO in spiked fresh plasma samples. For this purpose, seven different plasma samples spiked with CRO were prepared. The final concentrations of CRO in the spiked plasma were 0, 1, 25, 50, 100, 250, and 1000 μM. Fig. 4A and B shows the concentration-dependent SERS spectra of protein precipitated plasma samples (plasma/acetonitrile ratio of 1/3), as well as the

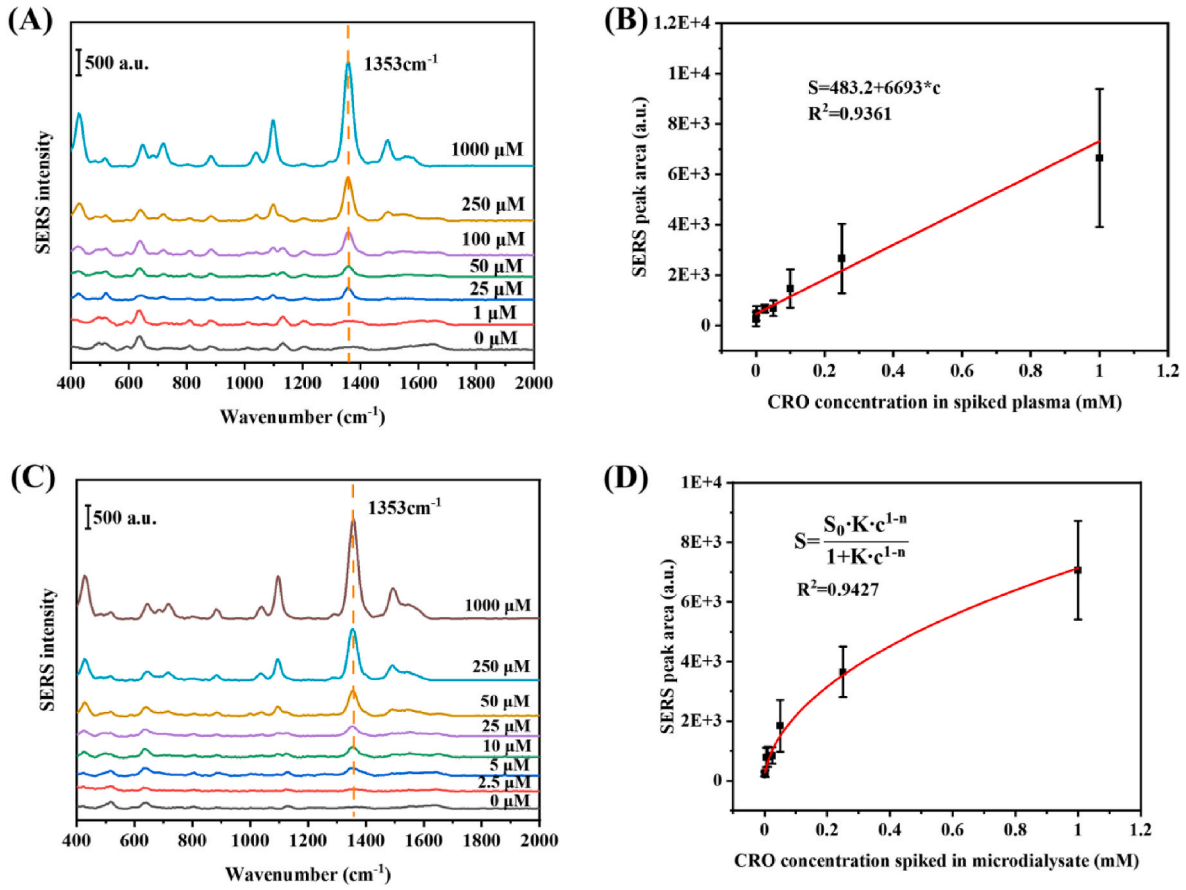

Fig. 4. (A) Mean SERS spectra of plasma samples spiked with different CRO concentrations after protein precipitation pre-treatment using acetonitrile (plasma/acetonitrile ratio 1/3). (B) Dependence of the SERS peak area at 1353 cm^{-1} on the CRO concentration between 1 μM and 1 mM using a linear fit (red line). (C) Average SERS spectra of microdialysate samples spiked with different CRO concentrations. (D) Dependence of the SERS peak area at 1353 cm^{-1} on the CRO concentration, ranging between 2.5 μM and 1 mM, using a Langmuir adsorption model fit (red line; parameters: S0 = 54183, K = 0.1516 and n = 0.5578).. (For an explanation of the color references in this legend, the reader is referred to the online version of this paper.)

respective peak area of the CRO marker mode at 1353 cm^{-1}, which increased as function of the CRO concentration spiked in plasma. The CRO marker band at 1353 cm^{-1} was clearly detectable down to 25 μM (equals 13.9 μg mL^{-1} CRO), a concentration that is meaningful for the detection of CRO in patient samples for TDM [49]. The R^2 value of the linear fit in Fig. 4B (S = 483.2 + 6693*c) was 0.9361, indicating the applicability of a linear fit model. The LOD is attributed to the 3σ level of the blank peak area divided by the slope of the fitted curve. In the case of protein precipitation as sample pre-treatment for plasma, an LOD of 94 μM was achieved. The relatively high LOD value, compared to the spectroscopic fingerprint detectable CRO concentration of down to 25 μM, was attributed to the presence of vibrational modes in the blank sample matrix occurring also in the region of the CRO marker band region. In fact, fresh plasma, even after the removal of proteins via protein precipitation, still contains small organic molecules or other interfering substances other than proteins. Thus, Raman bands due to the matrix background can be observed within the blank sample, i.e. 0 μM CRO. Due to the higher affinity of CRO towards the SERS substrate's surface compared to matrix molecules, interference with the CRO marker band at 1353 cm^{-1} was not observed at higher CRO concentrations. In addition, acetonitrile used for protein precipitation mediated detection of total antibiotic concentration in plasma, as CRO, which is highly bound to proteins in blood (90–95 % protein-bound at low concentrations [50]), was released from the proteins during the precipitation process.

As mentioned above only the free drug fraction is considered to be the pharmacologically active one. Thus, in TDM of critically ill patients with deviant PK parameters the therapeutic range can be better monitored with the free drug concentration than with the total drug concentration [51,52]. Among the different methods for free drug fraction sampling, microdialysis is an effective method that can be combined with near-patient POCT for semi-continuous on-line determination of protein-unbound target analyte concentrations [53]. In addition, with respect to SERS measurements, microdialysis reduces the complexity of sample matrix by depleting a high amount of matrix molecules such as proteins, which could potentially interfere with the SERS fingerprint information of the target analyte. Consequently, we tested microdialysates as sample matrix in potential TDM applications based on SERS by performing microdialysis with fresh plasma samples from healthy donor volunteers without CRO intake. In doing so, microdialysates depleted of peptides/proteins and other blood components with a molecular weight greater than 9 kDa were generated. Prior to the SERS measurements, we spiked microdialysates with CRO reaching various final CRO concentrations, i.e., 0, 2.5, 5, 10, 25, 50, 250 and 1000 μM. Fig. 4C and D shows the SERS spectra and the concentration dependency of the CRO marker modes peak areas. The SERS spectra plotted represent average spectra, calculated from 30 single spectra for each concentration. In comparison to protein precipitated plasma (Fig. 4A), the blank sample spectrum showed less dominant Raman modes after the application of microdialysis as sample pre-treatment. This can be explained by the fact that the mechanisms of the two pre-treatment processes differ significantly. Thus, whereas protein precipitation sample pre-treatment only efficiently reduces peptides/proteins in the sample, the physicochemical nature of the here applied microdialysis reduces also (larger) hydrophobic blood components (e.g., lipids), yielding in a less complex sample matrix. As the concentration of CRO spiked in microdialysates increased, the CRO marker modes became more prominent. The dependency of the SERS signal of the carboxyl vibration (integrated peak area at 1353 cm^{-1}) on the CRO concentration spiked in microdialysate samples was demonstrated by fitting the data to the Langmuir adsorption model (Fig. 4D). The fit illustrated as red line gave a R^2 of 0.9427 and the Langmuir isotherm parameters $S_0 = 54183$, K = 0.1516 and n = 0.5578. We attributed this Langmuir-like behavior to the fact that the interaction between the SERS substrate and the CRO molecule is much stronger than the attraction between CRO molecules itself [54,55].

Moreover, due to the less complex matrix composition, less interference of matrix molecules was expected when using microdialysate for SERS-based investigations. Due to the Langmuir behavior, we can conclude that the adsorbed CRO molecules were more likely generating a monolayer on the surface of the SERS substrate. In addition, it is known from the electromagnetic SERS enhancement theory that the SERS signal is mainly determined by the contribution of the analyte molecules closest to the metal surface [56]. The Raman signal of the first molecular layer can be directly enhanced, resulting in a Langmuir-like dependency as shown in Fig. 4D.

The LOD (3σ level) of CRO in microdialysates, calculated from the non-spiked blank samples, was 1.4 μM, which is equivalent to 0.83 μg mL^{-1}. Literature reports for a daily dose of 1 g CRO administered to an average adult a peak and trough plasma concentration of the protein-bound drug of 79–255 μg mL^{-1} and 15–45 μg mL^{-1}, respectively [3,49]. Considering that approx. 90–95 % of CRO is protein bound in plasma, free CRO concentrations in plasma are expected to range between 0.75 and 25.5 μg mL^{-1} [50]. Table 1 summarizes previous findings for estimation of CRO in biological matrices by SERS and compares them with our results, considering LODs as well as the measurement range within the SERS experiments. Here, the application of SERS for the determination of CRO in microdialysate samples presented itself competitive to other studies using less complex matrices and capable for semi-continuous TDM or PK analyses.

4. Conclusions

In conclusion, we successfully demonstrated the detection of the antibiotic CRO in fresh plasma and microdialysate by applying an own fabricated SERS substrate based on silicon nanowires decorated with silver nanostructures (Ag@SiNWs). In the case of fresh plasma as a biological matrix, we used a sample pre-treatment method for protein precipitation with acetonitrile. Most efficient protein precipitation and highest CRO marker mode (1353 cm^{-1}) SERS intensities were obtained with an optimized plasma/acetonitrile ratio of 1/3. By doing so, one has access to the total amount of the antibiotic in plasma in further experiments employing real clinical samples as the usually highly protein-bound antibiotic is released from matrix proteins by this sample pre-treatment. For TDM in patients with aberrant PK parameters, i.e. critically ill patients, the pharmacologically active free fraction of the antibiotic might be more informative than the total CRO concentration in plasma. Therefore, we performed SERS-based analysis on microdialysates, a sample matrix with less complex composition as in particular large biomolecules such as proteins are hindered to cross the membrane barrier in microdialysis. As less matrix molecules compete for free binding sites at the metallic SERS-active surface, the sensitivity of the SERS detection scheme could be increased and a LOD of 1.4 μM could be reached for CRO spiked in microdialysate samples. Thus, this

Table 1
An overview of the reported SERS studies on CRO detection.

Substrate	Matrix	Lowest detected concentration	SERS measurement range	Reference
AgNPs	urine sample	0.4 μg mL^{-1}	5–500 μg mL^{-1}	[36]
SERS sensing optical fiber	water	1 μM	10–10000 μM	[57]
CuNP	urine sample	7.5 μg mL^{-1}	50–500 μg mL^{-1}	[58]
AgNPs	urine sample	92 μg mL^{-1}	100–500 μg mL^{-1}	[59]
Ag@SiNWs	**fresh plasma**	**94 μM**	**1–1000 μM**	**Our work**
Ag@SiNWs	**microdialysate**	**1.4 μM**	**2.5–1000 μM**	**Our work**

work paves the way towards the estimation of antibiotics in clinical samples in terms of TDM.

CRediT authorship contribution statement

Chen Liu: Conceptualization, Investigation, Methodology, Writing – original draft, Writing – review & editing. **Célia Franceschini:** Conceptualization, Investigation, Writing – original draft. **Susanne Weber:** Conceptualization, Resources, Writing – review & editing. **Tony Dib:** Investigation. **Poting Liu:** Investigation. **Long Wu:** Conceptualization. **Edoardo Farnesi:** Investigation. **Wen-shu Zhang:** Conceptualization. **Vladimir Sivakov:** Funding acquisition, Supervision, Writing – review & editing. **Peter B. Luppa:** Conceptualization, Supervision, Writing – review & editing. **Jürgen Popp:** Funding acquisition, Supervision, Writing – review & editing. **Dana Cialla-May:** Conceptualization, Funding acquisition, Supervision, Writing – review & editing.

Declaration of competing interest

The authors declare that they have no known competing financial interests or personal relationships that could have appeared to influence the work reported in this paper.

Data availability

Data will be made available on request.

Acknowledgements

Funding of the project InfectoGnostics (13GW0096F) by BMBF, Germany, as well as the project 465289819 by DFG, Germany, is gratefully acknowledged. VS and PL gratefully acknowledge financial support by the German Research Foundation (DFG) under Grant No. 448666227 (SI1893/27-1). The authors give special thanks to Prof. Dr. Thomas Bocklitz and Dr. Oleg Ryabchykov (both Leibniz IPHT) for supporting the algorithm script in the program language R, Dr. Jan Dellith and Andrea Dellith in the Competence Center for Micro- and Nanotechnologies at Leibniz IPHT for supporting the characterization supporting, and Prof. Dr. Alois Bonifacio and Dr. Stefano Fornasaro (both University of Trieste, Italy) for helpful discussion.

Appendix A. Supplementary data

Supplementary data to this article can be found online at https://doi.org/10.1016/j.talanta.2024.125697.

References

[1] A. Jaworska, S. Fornasaro, V. Sergo, A. Bonifacio, Potential of surface enhanced Raman spectroscopy (SERS) in therapeutic drug monitoring (TDM). A critical review, Biosensors 6 (3) (2016).
[2] H.C. Ates, J.A. Roberts, J. Lipman, A.E.G. Cass, G.A. Urban, C. Dincer, On-site therapeutic drug monitoring, Trends Biotechnol. 38 (11) (2020) 1262–1277.
[3] S. Fornasaro, D. Cialla-May, V. Sergo, A. Bonifacio, The Role of Surface Enhanced Raman Scattering for Therapeutic Drug Monitoring of Antimicrobial Agents, Chemosensors, 2022.
[4] S.L. Bliese, M. Maina, P. Were, M. Lieberman, Detection of degraded, adulterated, and falsified ceftriaxone using paper analytical devices, Anal. Methods 11 (37) (2019) 4727–4732.
[5] S.G. Wicha, A.-G. Märtson, E.I. Nielsen, B.C.P. Koch, L.E. Friberg, J.-W. Alffenaar, I. K. Minichmayr, The international society of anti-infective pharmacology, from therapeutic drug monitoring to model-informed precision dosing for antibiotics, Clin. Pharmacol. Therapeut. 109 (4) (2021) 928–941, t.P.K.P.D.s.g.o.t.E.S.o.C.M.I. D.
[6] F. de Velde, J.W. Mouton, B.C.M. de Winter, T. van Gelder, B.C.P. Koch, Clinical applications of population pharmacokinetic models of antibiotics: challenges and perspectives, Pharmacol. Res. 134 (2018) 280–288.
[7] A. Huttner, S. Harbarth, W.W. Hope, J. Lipman, J.A. Roberts, Therapeutic drug monitoring of the β-lactam antibiotics: what is the evidence and which patients should we be using it for? J. Antimicrob. Chemother. 70 (12) (2015) 3178–3183.
[8] V. Avataneo, A. D'Avolio, J. Cusato, M. Cantù, A. De Nicolò, LC-MS application for therapeutic drug monitoring in alternative matrices, J. Pharmaceut. Biomed. Anal. 166 (2019) 40–51.
[9] S. Cairoli, R. Simeoli, M. Tarchi, M. Dionisi, A. Vitale, L. Perioli, C. Dionisi-Vici, B. M. Goffredo, A new HPLC–DAD method for contemporary quantification of 10 antibiotics for therapeutic drug monitoring of critically ill pediatric patients, Biomed. Chromatogr. 34 (10) (2020) e4880.
[10] S.E. Briscoe, B.C. McWhinney, J. Lipman, J.A. Roberts, J.P.J. Ungerer, A method for determining the free (unbound) concentration of ten beta-lactam antibiotics in human plasma using high performance liquid chromatography with ultraviolet detection, J. Chromatogr. B 907 (2012) 178–184.
[11] L. Herrera-Hidalgo, M.V. Gil-Navarro, S. Dilly Penchala, L.E. López-Cortes, A. de Alarcón, R. Luque-Márquez, L.F. López-Cortes, A. Gutiérrez-Valencia, Ceftriaxone pharmacokinetics by a sensitive and simple LC–MS/MS method: development and application, J. Pharmaceut. Biomed. Anal. 189 (2020) 113484.
[12] A.B. Kanu, Recent developments in sample preparation techniques combined with high-performance liquid chromatography: a critical review, J. Chromatogr. A 1654 (2021) 462444.
[13] M. Liszewska, B. Bartosewicz, B. Budner, B. Nasiłowska, M. Szala, J.L. Weyher, I. Dzięcielewski, Z. Mierczyk, B.J. Jankiewicz, Evaluation of selected SERS substrates for trace detection of explosive materials using portable Raman systems, Vib. Spectrosc. 100 (2019) 79–85.
[14] I.J. Jahn, A. Grjasnow, H. John, K. Weber, J. Popp, W. Hauswald, Noise sources and requirements for confocal Raman spectrometers in biosensor applications, Sensors 21 (2021) 5067.
[15] H. Wang, Z. Xue, Y. Wu, J. Gilmore, L. Wang, L. Fabris, Rapid SERS quantification of trace fentanyl laced in recreational drugs with a portable Raman module, Anal. Chem. 93 (27) (2021) 9373–9382.
[16] R. Xiao, L. Lu, Z. Rong, C. Wang, Y. Peng, F. Wang, J. Wang, M. Sun, J. Dong, D. Wang, L. Wang, N. Sun, S. Wang, Portable and multiplexed lateral flow immunoassay reader based on SERS for highly sensitive point-of-care testing, Biosens. Bioelectron. 168 (2020) 112524.
[17] J. Langer, D. Jimenez de Aberasturi, J. Aizpurua, R.A. Alvarez-Puebla, B. Auguié, J. J. Baumberg, G.C. Bazan, S.E.J. Bell, A. Boisen, A.G. Brolo, J. Choo, D. Cialla-May, V. Deckert, L. Fabris, K. Faulds, F.J. García de Abajo, R. Goodacre, D. Graham, A. J. Haes, C.L. Haynes, C. Huck, T. Itoh, M. Käll, J. Kneipp, N.A. Kotov, H. Kuang, E. C. Le Ru, H.K. Lee, J.-F. Li, X.Y. Ling, S.A. Maier, T. Mayerhöfer, M. Moskovits, K. Murakoshi, J.-M. Nam, S. Nie, Y. Ozaki, I. Pastoriza-Santos, J. Perez-Juste, J. Popp, A. Pucci, S. Reich, B. Ren, G.C. Schatz, T. Shegai, S. Schlücker, L.-L. Tay, K. G. Thomas, Z.-Q. Tian, R.P. Van Duyne, T. Vo-Dinh, Y. Wang, K.A. Willets, C. Xu, H. Xu, Y. Xu, Y.S. Yamamoto, B. Zhao, L.M. Liz-Marzán, Present and future of surface-enhanced Raman scattering, ACS Nano 14 (1) (2020) 28–117.
[18] D. Cialla, A. März, R. Böhme, F. Theil, K. Weber, M. Schmitt, J. Popp, Surface-enhanced Raman spectroscopy (SERS): progress and trends, Anal. Bioanal. Chem. 403 (1) (2012) 27–54.
[19] D. Cialla-May, X.S. Zheng, K. Weber, J. Popp, Recent progress in surface-enhanced Raman spectroscopy for biological and biomedical applications: from cells to clinics, Chem. Soc. Rev. 46 (13) (2017) 3945–3961.
[20] X.-S. Zheng, I.J. Jahn, K. Weber, D. Cialla-May, J. Popp, Label-free SERS in biological and biomedical applications: recent progress, current challenges and opportunities, Spectrochim. Acta Mol. Biomol. Spectrosc. 197 (2018) 56–77.
[21] L. Wu, C. Zhang, Y. Long, Q. Chen, W. Zhang, G. Liu, Food additives: from functions to analytical methods, Crit. Rev. Food Sci. Nutr. 62 (30) (2022) 8497–8517.
[22] L. Wu, W. Zhang, C. Liu, M.F. Foda, Y. Zhu, Strawberry-like SiO2/Ag nanocomposites immersed filter paper as SERS substrate for acrylamide detection, Food Chem. 328 (2020) 127106.
[23] L. Wu, H. Yan, G. Li, X. Xu, L. Zhu, X. Chen, J. Wang, Surface-imprinted gold nanoparticle-based surface-enhanced Raman scattering for sensitive and specific detection of patulin in food samples, Food Anal. Methods 12 (7) (2019) 1648–1657.
[24] C. Liu, L. Müller-Bötticher, C. Liu, J. Popp, D. Fischer, D. Cialla-May, Raman-based detection of ciprofloxacin and its degradation in pharmaceutical formulations, Talanta (2022) 123719.
[25] C. Liu, S. Weber, R. Peng, L. Wu, W.-s. Zhang, P.B. Luppa, J. Popp, D. Cialla-May, Toward SERS-based therapeutic drug monitoring in clinical settings: recent developments and trends, TrAC, Trends Anal. Chem. 164 (2023) 117094.
[26] I.J. Hidi, M. Jahn, M.W. Pletz, K. Weber, D. Cialla-May, J. Popp, Toward levofloxacin monitoring in human urine samples by employing the LoC-SERS technique, J. Phys. Chem. C 120 (37) (2016) 20613–20623.
[27] E.H. Koh, W.-C. Lee, Y.-J. Choi, J.-I. Moon, J. Jang, S.-G. Park, J. Choo, D.-H. Kim, H.S. Jung, A wearable surface-enhanced Raman scattering sensor for label-free molecular detection, ACS Appl. Mater. Interfaces 13 (2) (2021) 3024–3032.
[28] T. Yang, X. Guo, H. Wang, S. Fu, Y. wen, H. Yang, Magnetically optimized SERS assay for rapid detection of trace drug-related biomarkers in saliva and fingerprints, Biosens. Bioelectron. 68 (2015) 350–357.
[29] C. Andreou, M.R. Hoonejani, M.R. Barmi, M. Moskovits, C.D. Meinhart, Rapid detection of drugs of abuse in saliva using surface enhanced Raman spectroscopy and microfluidics, ACS Nano 7 (8) (2013) 7157–7164.
[30] A. Bonifacio, S. Dalla Marta, R. Spizzo, S. Cervo, A. Steffan, A. Colombatti, V. Sergo, Surface-enhanced Raman spectroscopy of blood plasma and serum using Ag and Au nanoparticles: a systematic study, Anal. Bioanal. Chem. 406 (9) (2014) 2355–2365.
[31] N.E. Markina, A.V. Markin, K. Weber, J. Popp, D. Cialla-May, Liquid-liquid extraction-assisted SERS-based determination of sulfamethoxazole in spiked human urine, Anal. Chim. Acta 1109 (2020) 61–68.

[32] M. Szultka, R. Kegler, P. Fuchs, P. Olszowy, W. Miekisch, J.K. Schubert, B. Buszewski, R.G. Mundkowski, Polypyrrole solid phase microextraction: a new approach to rapid sample preparation for the monitoring of antibiotic drugs, Anal. Chim. Acta 667 (1) (2010) 77–82.
[33] Y. Göksel, K. Zor, T. Rindzevicius, B.E. Thorhauge Als-Nielsen, K. Schmiegelow, A. Boisen, Quantification of methotrexate in human serum using surface-enhanced Raman scattering—toward therapeutic drug monitoring, ACS Sens. 6 (7) (2021) 2664–2673.
[34] O. Hayden, P.B. Luppa, J. Min, Point-of-care testing—new horizons for cross-sectional technologies and decentralized application strategies, Anal. Bioanal. Chem. 414 (10) (2022) 3161–3163.
[35] S. Weber, S. Tombelli, A. Giannetti, C. Trono, M. O'Connell, M. Wen, A.B. Descalzo, H. Bittersohl, A. Bietenbeck, P. Marquet, L. Renders, G. Orellana, F. Baldini, P. B. Luppa, Immunosuppressant quantification in intravenous microdialysate – towards novel quasi-continuous therapeutic drug monitoring in transplanted patients, Clin. Chem. Lab. Med. 59 (5) (2021) 935–945.
[36] N.E. Markina, I.Y. Goryacheva, A.V. Markin, Sample pretreatment and SERS-based detection of ceftriaxone in urine, Anal. Bioanal. Chem. 410 (8) (2018) 2221–2227.
[37] C. Li, W. Lin, Y. Shao, Y. Feng, Simultaneous determination of ternary cephalosporin solutions by Raman spectroscopy, Chin. Opt Lett. 11 (12) (2013), 123001-123001.
[38] E.C. Le Ru, S.A. Meyer, C. Artur, P.G. Etchegoin, J. Grand, P. Lang, F. Maurel, Experimental demonstration of surface selection rules for SERS on flat metallic surfaces, Chem. Commun. 47 (13) (2011) 3903–3905.
[39] M. Moskovits, J.S. Suh, Surface selection rules for surface-enhanced Raman spectroscopy: calculations and application to the surface-enhanced Raman spectrum of phthalazine on silver, J. Phys. Chem. 88 (23) (1984) 5526–5530.
[40] M.R. Gonçalves, F. Enderle, O. Marti, Surface-enhanced Raman spectroscopy of dye and thiol molecules adsorbed on triangular silver nanostructures: a study of near-field enhancement, localization of hot-spots, and passivation of adsorbed carbonaceous species, J. Nanotechnol. 2012 (2012) 173273.
[41] J.H. Parker, D.W. Feldman, M. Ashkin, Raman scattering by silicon and germanium, Phys. Rev. 155 (3) (1967) 712–714.
[42] S. Patze, U. Huebner, K. Weber, D. Cialla-May, J. Popp, TopUp SERS substrates with integrated internal standard, Materials 11 (2) (2018).
[43] P. Li, X. Wang, H. Li, X. Yang, X. Zhang, L. Zhang, Y. Ozaki, B. Liu, B. Zhao, Investigation of charge-transfer between a 4-mercaptobenzoic acid monolayer and TiO2 nanoparticles under high pressure using surface-enhanced Raman scattering, Chem. Commun. 54 (49) (2018) 6280–6283.
[44] X. Dong, J. Zhou, X. Liu, D. Lin, L. Zha, Preparation of monodisperse bimetallic nanorods with gold nanorod core and silver shell and their plasmonic property and SERS efficiency, J. Raman Spectrosc. 45 (6) (2014) 431–437.
[45] D.V. Yakimchuk, V.D. Bundyukova, J. Ustarroz, H. Terryn, K. Baert, A. L. Kozlovskiy, M.V. Zdorovets, S.A. Khubezhov, A.V. Trukhanov, S.V. Trukhanov, L.V. Panina, G.M. Arzumanyan, K.Z. Mamatkulov, D.I. Tishkevich, E.Y. Kaniukov, V. Sivakov, Morphology and microstructure evolution of gold nanostructures in the limited volume porous matrices, Sensors 20 (2020) 4397.
[46] H.A. Krebs, Chemical composition of blood plasma and serum, Annu. Rev. Biochem. 19 (1) (1950) 409–430.
[47] T. Cedervall, I. Lynch, S. Lindman, T. Berggård, E. Thulin, H. Nilsson, K.A. Dawson, S. Linse, Understanding the nanoparticle–protein corona using methods to quantify exchange rates and affinities of proteins for nanoparticles, Proc. Natl. Acad. Sci. USA 104 (7) (2007) 2050–2055.
[48] S. Yıldırım, K. Fikarová, V. Pilařová, L. Nováková, P. Solich, B. Horstkotte, Lab-in-syringe automated protein precipitation and salting-out homogenous liquid-liquid extraction coupled online to UHPLC-MS/MS for the determination of beta-blockers in serum, Anal. Chim. Acta 1251 (2023) 340966.
[49] A.A. Pollock, P.E. Tee, I.H. Patel, J. Spicehandler, M.S. Simberkoff, J.J. Rahal, Pharmacokinetic characteristics of intravenous ceftriaxone in normal adults, Antimicrob. Agents Chemother. 22 (5) (1982) 816–823.
[50] A.C. Popick, W.G. Crouthamel, I. Bekersky, Plasma protein binding of ceftriaxone, Xenobiotica 17 (10) (1987) 1139–1145.
[51] M. Schleibinger, C.L. Steinbach, C. Töpper, A. Kratzer, U. Liebchen, F. Kees, B. Salzberger, M.G. Kees, Protein binding characteristics and pharmacokinetics of ceftriaxone in intensive care unit patients, Br. J. Clin. Pharmacol. 80 (3) (2015) 525–533.
[52] T.M.J. Ewoldt, S. Bahmany, A. Abdulla, A.E. Muller, H. Endeman, B.C.P. Koch, Plasma protein binding of ceftriaxone in critically ill patients: can we predict unbound fractions? J. Antimicrob. Chemother. 78 (4) (2023) 1059–1065.
[53] B. Seyfinejad, S.A. Ozkan, A. Jouyban, Recent advances in the determination of unbound concentration and plasma protein binding of drugs: analytical methods, Talanta 225 (2021) 122052.
[54] X. Zhang, C.R. Yonzon, R.P. Van Duyne, Nanosphere lithography fabricated plasmonic materials and their applications, J. Mater. Res. 21 (5) (2006) 1083–1092.
[55] K.V. de Oliveira, J.C. Rubim, Surface-enhanced Raman spectroscopy of molecules adsorbed on silver nanoparticles dispersed an agarose gel and their adsorption isotherms, Vib. Spectrosc. 86 (2016) 290–301.
[56] S. Schlücker, Surface-enhanced Raman spectroscopy: concepts and chemical applications, Angew. Chem. Int. Ed. 53 (19) (2014) 4756–4795.
[57] D. Gao, X. Yang, P. Teng, Z. Liu, J. Yang, D. Kong, J. Zhang, M. Luo, Z. Li, F. Tian, L. Yuan, Optofluidic in-fiber integrated surface-enhanced Raman spectroscopy detection based on a hollow optical fiber with a suspended core, Opt. Lett. 44 (21) (2019) 5173–5176.
[58] N.E. Markina, S.N. Ustinov, A.M. Zakharevich, A.V. Markin, Copper nanoparticles for SERS-based determination of some cephalosporin antibiotics in spiked human urine, Anal. Chim. Acta 1138 (2020) 9–17.
[59] N.E. Markina, A.V. Markin, Application of aluminum hydroxide for improvement of label-free SERS detection of some cephalosporin antibiotics in urine, Biosensors 9 (3) (2019).